ADVANCED FUNCTIONAL MATERIALS
www.afm-journal.de

Inorganic Solids of CdSe Nanocrystals Exhibiting High Emission Quantum Yield

*Elena Khon, Scott Lambright, Dmitry Khon, Bryan Smith, Timothy O'Connor, Pavel Moroz, Martene Imboden, Geoffrey Diederich, Cesar Perez-Bolivar, Pavel Anzenbacher, and Mikhail Zamkov**

A general strategy for the assembly of all-inorganic light-emitting nanocrystal films with emission quantum yield in the 30–52% range is reported. The present methodology relies on solution-processing of CdSe nanocrystals into a crystalline matrix of a wide band gap semiconductor (CdS, ZnS), which replaces the original molecular ligands on nanocrystal surfaces with an inorganic medium. Such matrices efficiently protect nanoparticles from the surrounding environment and preserve the quantum confinement of electrical charges in embedded CdSe NCs. In addition to strong emission, fabricated films show excellent thermal and chemical stability, and a large refractive index, which avails their integration into emerging solid-state nanocrystal devices, including light-emitting diodes, solar concentrators, and quantum dot lasers.

1. Introduction

Colloidal semiconductor nanocrystals (NCs) are emerging as a promising class of nanomaterials for the development of solid state optical applications. The quantum confinement of charges in NCs allows for continuous tunability of the emission color *via* the nanoparticle size, while the ease of colloidal manipulation of NC solutions enables a low-cost deposition of these nanostructures into thin-film and waveguide geometries. Owing to these advantages, the integration of semiconductor NCs into solid state optical applications has been actively explored in the last decade leading to the demonstration of important functional devices, such as light-emitting diodes (LEDs)[1–9] and quantum dot lasers.[10–18] While the performance of these first prototypes was still inferior to those of more conventional techniques utilizing organic polymers[19] or epitaxial quantum dots,[20] a unique combination of low-cost, size-tunable properties, and rigid inorganic lattice structure associated with semiconductor NCs is expected to secure their important role in the development of next-generation light-emitting materials.

A significant challenge for optical applications of colloidal NCs concerns their integration into transparent host matrices compatible with solid-state microelectronic technologies. Ideally, these matrices have to preserve the low size-dispersion and high emission quantum yield of incorporated NCs, exhibit good thermal and chemical stability, and possess a high refractive index in order to be pertinent for utilization in waveguides. Earlier incorporation techniques relying on the inclusion of semiconductor NCs into organic polymer mixes[21–24] were reasonably successful in converting nanoparticle solutions into device-compatible films, but had suffered from relatively low nanoparticle volume loading (filling factor), as well as polymer/semiconductor phase separation. The employment of sol-gel titania matrices[25,26] in lieu of polymers has resolved many of these issues, as was evidenced by an improved thermal stability and high packing density of TiO_x-incorporated NC films. Titania matrices have also enabled an enhanced refractive index of the NC film approaching 1.8.[25] Nevertheless, the emission quantum yield of NC-titania assemblies was still below the 15% margin, a significant drop from the 60–85%[27] yield of NCs in their colloidal form. Furthermore, the chemical stability of these materials was compromised by the hydrophilic composition of titania films, which showed degradation in the presence of moisture, water, or alcohols.

One aspect common to many existing strategies for matrix integration of semiconductor NCs is the employment of molecular ligands on surfaces of incorporated nanoparticles as a main mechanism for preserving the quantum confinement of charges. Indeed, despite the variety of reported encapsulation approaches utilizing matrix materials such as clay,[28] metal-alkoxide derived ormosils,[29] titania,[25] β-cyclodextrin,[30] or PMMA,[23] the emission of embedded NCs was still enabled

E. Khon, Dr. D. Khon, P. Moroz, Prof. M. Zamkov
The Center for Photochemical Sciences
and Department of Physics
Bowling Green State University
Bowling Green, OH 43403, USA
E-mail: zamkovm@bgsu.edu
S. Lambright, B. Smith, T. O'Connor, G. Diederich
Department of Physics
Bowling Green State University
Bowling Green, OH 43403, USA
Dr. C. Perez-Bolivar, Prof. P. Anzenbacher
The Center for Photochemical Sciences and Department of Chemistry
Bowling Green State University
Bowling Green, OH 43403, USA
M. Imboden
Department of Chemistry
Bowling Green State University
Bowling Green, OH 43403, USA

DOI: 10.1002/adfm.201200939

exclusively by the passivating action of surface ligands; either original long-chain fatty acids, inorganic metal chalcogenide complexes,[31] or alcohol-terminated amines. This reliance on surface molecules for enabling the fluorescence of NCs in matrices presents a number of intrinsic limitations. First, the tendency of surface ligands to desorb from NCs as a result of thermal or electrical stimulation inevitably compromises the stability of NC emission in the film, regardless of the stability of the matrix medium. For instance, state-of-the-art LED devices utilizing fully inorganic electron and hole transport layers still integrate organically capped NCs,[9] which may cause potential stability issues in the long-term operation of these assemblies. Second, the volume of the low-refractive-index organic shell formed by the surface ligands is comparable to the nanocrystal volume, which inevitably lowers the overall refracting index of the film, making it less suitable for wave-guide applications. Third, most organic ligands that enable the high emission yield in semiconductor NCs are subject to photodegradation caused by the exposure of ligands to ultraviolet radiation[32] which, poses stability concerns.

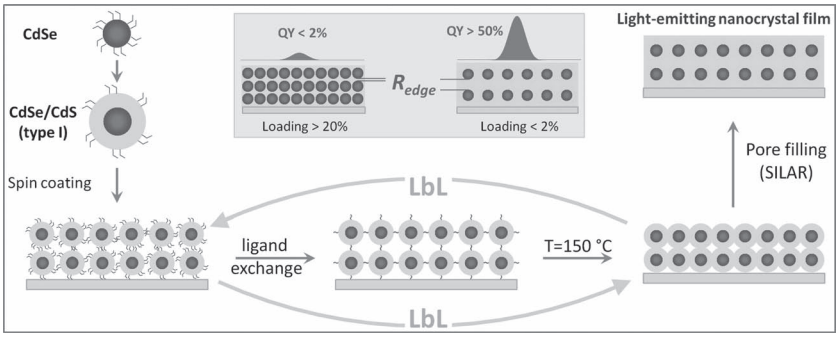

Figure 1. Illustration of the general strategy for encapsulation of chemically-grown semiconductor NCs into all-inorganic (SMENA) films. CdSe NCs are first capped with a shell of a matrix semiconductor (CdS or ZnS) using colloidal synthesis. The resulting core/shell NCs are then deposited into a film, capped with thermally degradable surface ligands and annealed at 150 °C, which expels the organic materials and promotes crystallographic fusion of the shells. The pores of the resulting solid are then filled with the additional CdS (ZnS) material using SILAR technique.

Here we address the issues of low emission yield and chemical instability of NC matrices through the use of ligand-free encapsulation of colloidal nanocrystals within an all-inorganic crystalline solid. The present technique builds upon a recently reported semiconductor matrix embedded nanocrystal array (SMENA) approach,[33] which allows for a gap-free inclusion of colloidal NCs into host matrices of wide band gap semiconductors. In particular, we demonstrate that such matrices can provide a substantial potential barrier to electrical charges in embedded nanoparticles, giving rise to strong NC emission. More importantly, due to heteroepitaxial bonding at nanocrystal/matrix interfaces, the matrix semiconductor efficiently protects NC surfaces from heat and oxidation, improving the overall stability of the film. In this work, we employ either CdS or ZnS semiconductors to encapsulate an array of equally-spaced CdSe NCs, such that the resulting solids show excellent thermal and chemical stability, high refractive index (n ≈ 1.9–2.2), and a filling factor continuously tunable in the 2–30% range. This combination of characteristics cannot be easily obtained simply by anealing a blend of CdSe/CdS and ZnS nanocrystals, in which case the interparticle distance in the film is poorly controlled.[34] Perhaps, the most appealing aspect of the present methodology is the demonstrated co-existence of inorganic surface capping and strong emission of embedded NCs with the associated fluorescence quantum yield in the 30–52% range.

2. Results and Discussion

The heteroepitaxial inclusion of colloidal CdSe NCs into semiconductor matrices was performed using a scheme outlined in **Figure 1**. First, CdSe NCs grown by standard hot-injection methods[35] were, overcoated with the shell of CdS or stoichiometrically graded $Zn_xCd_{1-x}S$/ZnS semiconductors. The resulting core/shell NCs were then spincoated onto a substrate, and subjected to *in situ* ligand exchange aimed to replace original surfactants (primarily oleic acid and tri-n-octylphosphine) with thermally degradable 3-mercaptopropionic acid (MPA) or formic acid (FA) molecules. Layer-by-layer (LbL)[36] deposition was used at this stage to avoid cracking of the film. Subsequently, a layer of MPA-capped CdSe/CdS ($CdSe/Zn_xCd_{1-x}S$/ZnS) core/shell NC film was heated under argon to 140–150 °C which induced a thermal removal of the organic phase and promoted a partial crystallographic fusion of neighboring shells. At these temperatures, sintering of CdSe cores was not observed. The resulting all-inorganic solids consisting of CdSe NCs embedded into CdS (or graded $Zn_xCd_{1-x}S$/ZnS) matrices were then exposed to several cycles of successive ionic layer adsorption and reaction (SILAR),[37,38] intended to fill the remaining void areas in the solid with additional CdS (or ZnS). It is important to note that the pore-filling step does not increase the interparticle separation between CdSe NCs, which is determined solely by the thickness of the shell in precursor nanoparticles. This maintains an equal edge-to-edge distance (R_{egde}) between embedded CdSe NCs which, along with the band gap of the matrix semiconductor, determines the resulting optoelectronic properties of the solid. For instance, NC films utilizing short R_{edge} distances (<0.7 nm) were shown[33] to support strong electrical coupling between neighboring NCs, evidenced through an excellent electrical conductance and a complete suppression of the band-gap fluorescence. In this work, the electrical coupling between neighboring nanocrystals was purposefully decreased by using large values of R_{egde} (≈0.8–10 nm), which resulted in the suppression of interparticle charge tunneling, leading to strong band gap emission.

The architecture of fabricated CdSe/CdS (CdSe/ZnS) SMENA films presents several distinct advantages for the development of NC optical applications. First, the encapsulation of light-emitting CdSe NCs within a matrix of a wide gap semiconductor provides an elegant approach for capping NC surfaces with a layer of inorganic material exhibiting a greater degree of tolerance to heat and oxidation than traditional molecular ligands.

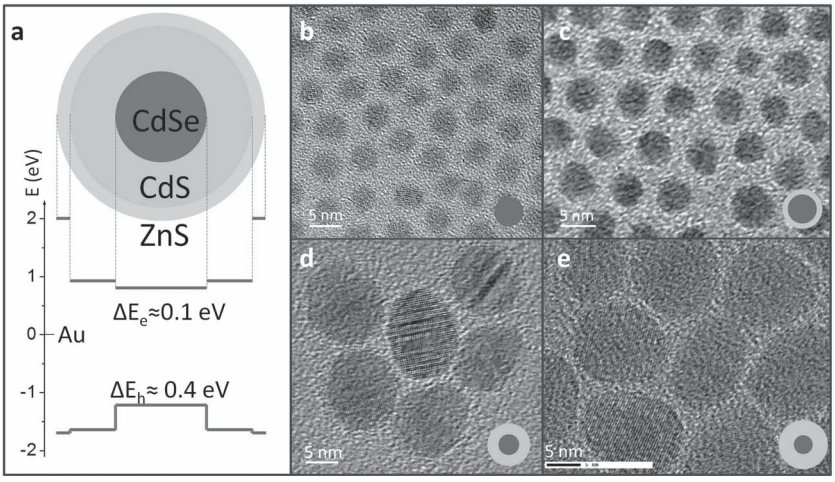

Figure 2. (a) The energy diagram showing relative offsets of electron and hole energy levels at core/shell interfaces. Zero of the energy scale corresponds to the ionization potential of gold. (b–e) Transmission electron microscope (TEM) images of CdSe (b) and CdSe/CdS(b-d) core/shell NCs, used for fabrication of SMENA solids.

Such improved stability of matrix-encapsulated NC solids is particularly important for the development of heat-intensive applications, including active lasing components, luminescent solar concentrators,[39] and LEDs. Second, since the volume of fabricated films is filled at an 80–85% level with a high-*n* semiconductor material, such as CdS or ZnS, the overall refractive index of the film is increased in comparison with commonly used polymer or titania matrices. Third, the SMENA architecture allows for a *continuous* optimization of the balance between the filling factor of the solid and the FL quantum yield (QY) of incorporated CdSe NCs (tunable *via* interparticle spacing), a task which is difficult to perform using methodologies that rely on amorphous metal chalcogenide matrices.[31,40] As this study demonstrates, a 52% emission yield can be realized for films with an associated filling factor of <2%, while high filling factors (>20%) tend to lower the emission yield to 1–3%.

A detailed description of the steps involved in the colloidal synthesis of CdSe and CdSe/CdS NCs is provided in the Experimental section. Briefly, nearly monodisperse CdSe NCs (Δd < 6%, **Figure 2**b) were fabricated according to a methodology that was previously reported.[35,38] Subsequently, a 1–15 monolayer (ML) shell of CdS was grown onto CdSe NCs (Figures 2c-2e) using an "accelerated" shell deposition technique developed in this work. The key advantage of this procedure is that it requires less than 15 min for the complete growth of the ~15 ML shell, which is substantially faster than previously reported SILAR-based synthesis of "giant" NCs, which can take up to 78 h for the same shell thickness.[41] The trade-off for such significant gain in the growth speed is the reduced control over the number of grown monolayers. In the present approach, the shell thickness can be determined only after the reaction is completed by means of TEM analysis of NC specimens, while the previously reported SILAR-based technique allows for a strict control of the number of grown MLs. Nevertheless, the size dispersion of core/shell NCs grown using the "accelerated" methodology was comparable to that of a SILAR-based method. As evident from Figure 2c, thin-shelled NCs (shell thickness, H ≈ 0.6 nm or 0.17 MLs) were fairly monodisperse (Δd ≈ 7.6%), while large-diameter nanoparticles (H >3 nm, Figures 2d,e) exhibited an average size dispersion of 10–12%. According to the x-ray powder diffraction spectra (XRD) in Figure SI1 (Supporting information), the shell grew in the wurtzite crystallographic phase.

According to a high-resolution (HR) TEM image of a typical CdSe/CdS core/shell structure (Figure SI2), the crystalline lattice of the CdS shell was nearly free of defects, which was attributed to a relatively low lattice stress at the interface of CdSe and CdS crystal phases (strain ≈ 4.3%). The existance of a relatively low strain between CdSe and CdS lattices has also motivated the use of CdS as a stress-relief layer prior to the growth of the ZnS shell. Indeed, the direct deposition of more than 4 MLs of ZnS onto CdSe is known to suppress the band gap emission due to the strain-related defect formation, which is best described as the formation of unpassivated cationic/anionic sites (dangling bonds) along the interface of CdSe and ZnS materials, meanwhile deposition of the "graded" $CdS/Cd_xZn_{1-x}S/ZnS$ shell reduces interfacial stress and enables a substantial localization of the charges in the core domain without compromising the emission yield. Judging by the slightly elongated shape of most specimens (Figures 2d,e; SI2), the expansion of the shell along the 001 axis of the wurtzite crystal structure occurred at a faster rate than along 010 and 100 crystallographic directions, which is consistent with previous reports.[42,43] To minimize elongation and keep the shape of NCs close to spherical, a strict control over the concentration of CdSe NCs in the shell growth solution was established (see Experimental Section for details).

The character of electron-hole localization in CdSe/CdS core/shell NCs was substantiated based on steady-state optical measurements of excited state transitions in the CdSe domain. According to **Figure 3**a, growth of the CdS shell onto CdSe NCs resulted in a red-shift of the emission peak from 585 to 630 nm, attributed to a partial delocalization of the electronic wavefunctions into the CdS shell.[44] This behavior is consistent with a type I band edge alignment in a core/shell system for which both electrons and holes are confined to the core portion of the structure by the potential barrier of the shell, as illustrated in Figure 2a. Realization of this type of carrier confinement in CdSe/CdS NCs is an important prerequisite for the development of light-emitting solids since it forces the localization of both charges within CdSe domains of the CdSe/CdS film, such that the probability of finding electrons or holes at defect-rich surfaces and interfaces of fused core/shell NCs becomes minimal. We note that for small-diameter CdSe NCs, the CdSe/CdS system can exhibit quasi type II band edge alignment,[45] in which case electrons become delocalized over the entire volume of the heteronanocrystal,[46] potentially suppressing the emission of the core in a film geometry. To avoid this scenario, CdSe NCs with diameters greater than 4.0 nm were used. According to Figure 3a, the growth of the CdS shell was accompanied by

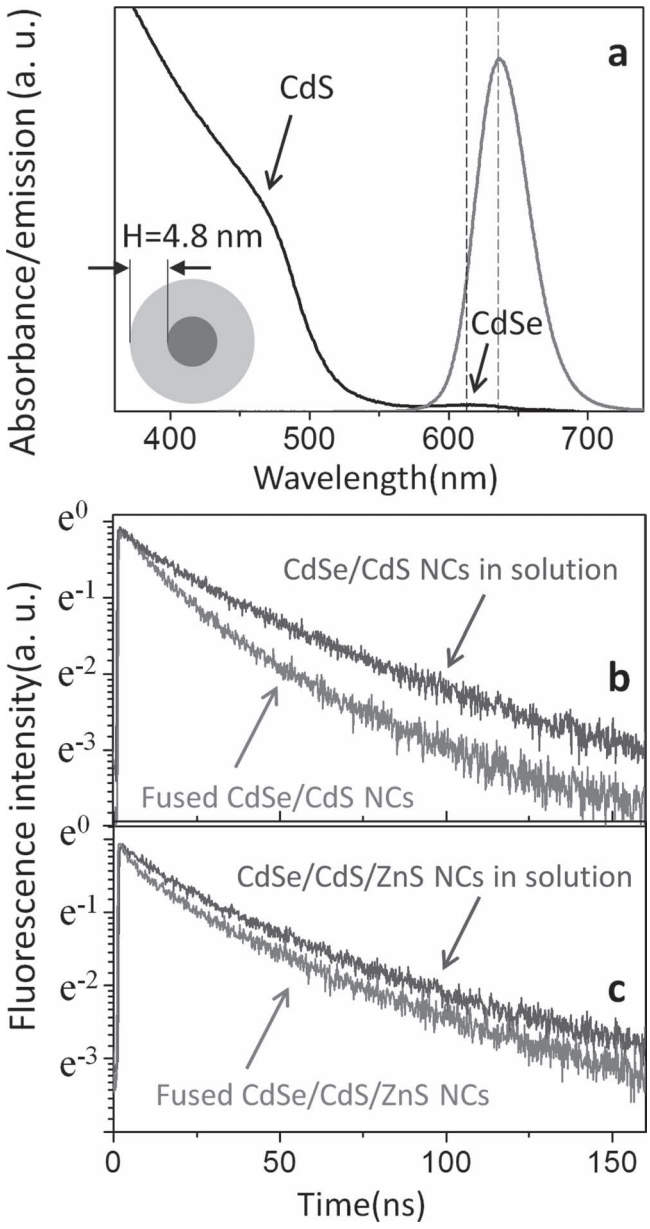

Figure 3. (a) The emission and absorption profiles of 13.7-nm CdSe/CdS core/shell NCs in toluene. The shell thickness was approximately 4.8 nm or 13 ML (see Figure 2e), and the core diameter – 4.0 nm. (b) Comparison of the fluorescence intensity decay traces between colloidal 13.7-nm CdSe/CdS core/shell NCs (blue curve) and CdSe/CdS solids fabricated by fusing 13.7-nm CdSe/CdS core/shell NCs into a solid (red curve). A shortened lifetime for the latter case indicates some degree of electrical coupling between charges in adjacent CdSe NCs. (c) Fluorescence intensity decay traces of colloidal (blue curve) and interfused (red curve) 14.2-nm CdSe/CdS/ZnS core/shell NCs, grown by adding 0.25 nm of ZnS shell onto nanoparticles in (a). The decay times are closer in this case due to weaker coupling of CdSe charges across several MLs of the ZnS barrier.

the enhancement of the absorption amplitude corresponding to the CdS band gap transition ($\lambda \approx 460$ nm), such that for core/shell NCs with 13 monolayers of the CdS shell (H ≈ 5 nm) the ratio of CdS absorbance (at $\lambda = 460$ nm) to that of CdSe ($\lambda = 620$–630 nm) was greater than 14. Expectedly, the CdS excitonic features of thick-shelled NCs were nearly washed out (see Figure 3a) reflecting the shell's growth beyond the CdS exciton Bohr radius (R = 2.9 nm).[47]

Crystallographic fusion of colloidal CdSe/CdS core/shell NCs into all-inorganic solids was performed using a three step procedure. First, a thin layer of organically-capped NCs in octane was spincoated onto a microscope glass slide or ITO-covered glass. In the next step, the original surface ligands on CdSe (hexadecylamine (HDA), octadecylphosphonic acid (ODPA), and TOP) were replaced with thermally degradable molecules, such as MPA (T_{bp} = 111 °C) or formic acid (FA, T_{bp} = 101 °C), which was achieved by exposing spincoated solids to a solution of a new ligand. Several layer-by-layer (LbL) cycles[48] were used at this stage to facilitate a replacement of original surfactants with MPA (FA) and to prevent cracking of the film due to the reduction in volume. The disappearance of MPA vibrational transitions in Fourier transform infrared spectroscopy (FTIR) spectra of resulting nanocrystal solids confirmed a near-complete removal of molecular surfactants from the film (Figure SI3).

The annealing step activates the fusion of core/shell NCs into a porous solid with the combined volume of unfilled areas equaling ≈ 45%, as determined from the average value of the film's refractive index (n ≈ 1.83, measured with PhE-101ellipsometer). Here we assume that a completely filled CdSe/CdS film is expected to have a refractive index approaching that of a CdSe/CdS combination (n ≈ 2.47 at $\lambda = 632.8$ nm), such that the presence of void regions in the solid lowers the refractive index proportionally to the unfilled volume. Notably, the existence of void regions renders the film less suitable for waveguiding applications, whereas the presence of unpassivated CdS (ZnS) matrix surfaces causes a high density of dangling bonds, which, despite a substantial energy barrier separating CdSe charges from matrix surfaces, can still trap carriers. To reduce the volume of void regions in the film, annealed NC solids were treated with additional matrix material (CdS, ZnS), which was introduced into the pores of fused core/shell NCs *via* SILAR technique. This step results in partial filling of gaps in SMENA, giving rise to monolithic solids with identifiable CdS lattice structure (see **Figures 4**c-e). The degree of filling was determined from the enhancement in the refractive index of in-filled films. For instance, four SILAR cycles were found to increase the average n from 1.83 to ≈2.1, which corresponds to the enhancement in the fraction of the semiconductor-filled region from 55 to 75%, while 6 SILAR cycles resulted in n ≈ 2.2 (80% filled, 20% void). Such efficient filling of void regions in the solid is consistent with the previously observed ability of Cd and S ions to penetrate through nanoparticle films, as was exemplified in recent experiments on porous TiO_2 films (3–4 μm in thickness), in which CdS material was deposited throughout the entire depth of the film (judging by the even coloration of both the front and the back sides of the opaque Degussa TiO_2 layer on glass).[49]

An important parameter underlying the light-emitting characteristics of fabricated CdSe solids is the degree of electrical coupling between adjacent CdSe NCs in the matrix. For instance, the presence of strong interparticle coupling, resulting from a significant overlap of excited state wave functions across neighboring NCs, results in the suppression of fluorescence due to charge tunneling. Conversely, for solids with weak CdSe–CdSe

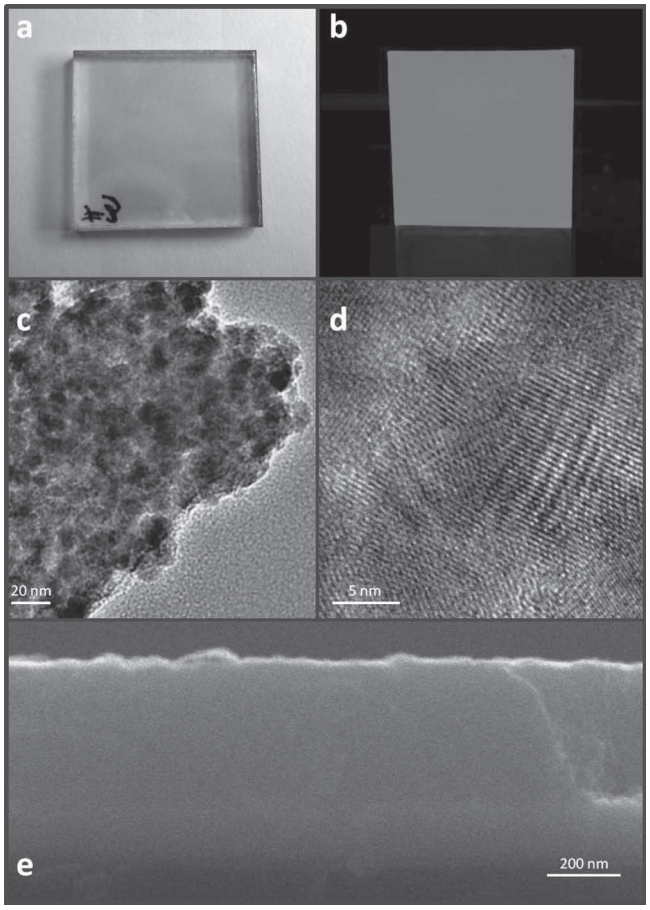

Figure 4. (a) CdSe/CdS SMENA film developed on glass. (b) The emission under ultraviolet excitation. (c-d) TEM images of SMENA fragments transferred from the glass substrate onto a TEM grid. The high-resolution image in (d) shows characteristic lattice fringes indexed to CdS. (e) Scanning electron microscope (SEM) image of the CdSe/CdS SMENA film on FTO-covered glass.

coupling, such tunneling mechanism (as well as charge trapping at matrix surfaces) is strongly inhibited due to carrier localization, which forces the excited charges to decay *via* the 1S(e)-1S(h) radiative channel. The strength of the CdS potential barrier to electrical charges in CdSe is well illustrated by probing the effect of surface molecules on the amplitude FL emission in core/shell NCs. It is well known that the replacement of the original bulky ligands on CdSe NCs with hydrophilic mercaptoundecanoic acid (MUA) molecules quenches the CdSe emission due to NC-to-ligand hole transfer.[50–52] Contrary to CdSe NCs, the FL quantum yield of aqueous CdSe/CdS core/shell NCs (H = 4.8 nm) was retained upon ligand exchange (see Figure SI4), confirming a negligible rate of the CdSe-to-MUA hole transfer across the 4.8-nm CdS shell.

To examine the dependence of the emission intensity and FL lifetime of CdS-encapsulated CdSe NC films on the average edge-to-edge distance between NCs (R_{edge}), we first consider weakly coupled NC solids ($R_{edge} \approx 9.6$ nm), fabricatied *via* the crystallographic fusion of 13.7-nm CdSe/CdS core/shell NCs. According to Figure 3b, the FL lifetime of CdSe/CdS NCs in the film is very close to that of isolated CdSe/CdS NCs indicating a negligibly slow charge transfer between neighboring NCs. Likewise, the high FL quantum yield (60–80%) of large-diameter CdSe/CdS NCs was reduced by approximately a factor of two upon transfer of these nanoparticles into an all-inorganic film, showing QY values of 30–43%. This data strongly suggests that a 4.8-nm CdS shell serves as a sufficient potential barrier to both electrons and holes residing within the 4.0-nm CdSe NCs, such that the probability of finding either charge carrier on the surface of a core/shell NC is negligible. The emission yield of CdSe solids was further improved to 45–52% upon adding just a few monolayers of a wide band gap ZnS shell onto 13.7-nm CdSe/CdS core/shell NCs. The increased emission QY reflects the reduction in the interparticle charge-coupling across the ZnS barrier, as was corroborated by the enhanced FL lifetime of charges in CdSe/CdS/ZnS solids (see Figure 3c).

The high emission yield of SMENA films (up to 52%) utilizing R_{edge} value of ≈10 nm comes at the price of a low filling factor, which did not exceed 2% for this case. To find a suitable compromise between the nanoparticle loading and the emission yield of the solid we have explored several film morphologies representing progressive enhancement of the interparticle distance R_{edge}. The results are summarized in **Figure 5**, which compares the emission lifetime of CdS-encapsulated NC films with R_{edge} values of 6.3, 2.3, and 0.8 nm, and respective CdSe loading percentages of 3.1%, 13%, and 31%. Due to the reduction in the interparticle distance, the emission lifetimes of CdSe domains in the film are now noticeably shorter than their respective values in solutions. This is attributed to the decreased width of the potential barrier separating CdSe NCs in the solid. For instance, when $R_{edge} \approx 10$ nm, the FL lifetime of NCs in solution exceeds that of a film by a factor of 1.34 (1.58 in case of all CdS matrix), whereas for $R_{edge} = 0.8$ nm, the lifetime of NCs in solution becomes 27 times greater than that of a solid. Among the factors limiting the FL lifetime and associated FL quantum yield of CdSe NCs in the film geometry are the processes of interparticle charge tunneling and carrier trapping on surfaces. The effect of the latter had been confirmed through the exchange of original ligands on thin-shelled CdSe/CdS NCs (H = 3 MLs) with electron-donating MUA molecules, in which case the emission lifetime of NCs in water dropped down to 4.6 ns, indicating that a 3ML shell does not provide a sufficient potential barrier between excited holes in CdSe and surface states of the CdS shell.

The summary of optical properties for CdS-encapsulated CdSe NC films corresponding to descending values of R_{edge} is provided in **Table 1** (optical properties of ZnS-encapsulated CdSe NC solids are discussed below). One apparent trend revealed by these measurements is an expected reduction in the emission yield of CdSe NCs with decreasing R_{edge}. This behavior is consistent with the Wentzel-Kramers-Brillouin (WKB) approximation[53] of interparticle coupling in the solid, expressed as

$$\beta \approx h\nu \exp\left(-2\left(2m* \Delta E/\hbar\right)^{1/2} R_{edge}\right) \quad (1)$$

where β is the energy of interparticle coupling, ΔE is the height of the potential barrier between electrons or holes in adjacent NCs, ν is a constant with the units of frequency, $m*$ is the carrier effective mass, and R_{edge} is the shortest edge-to-edge distance between the adjacent NCs in the film. Within the above

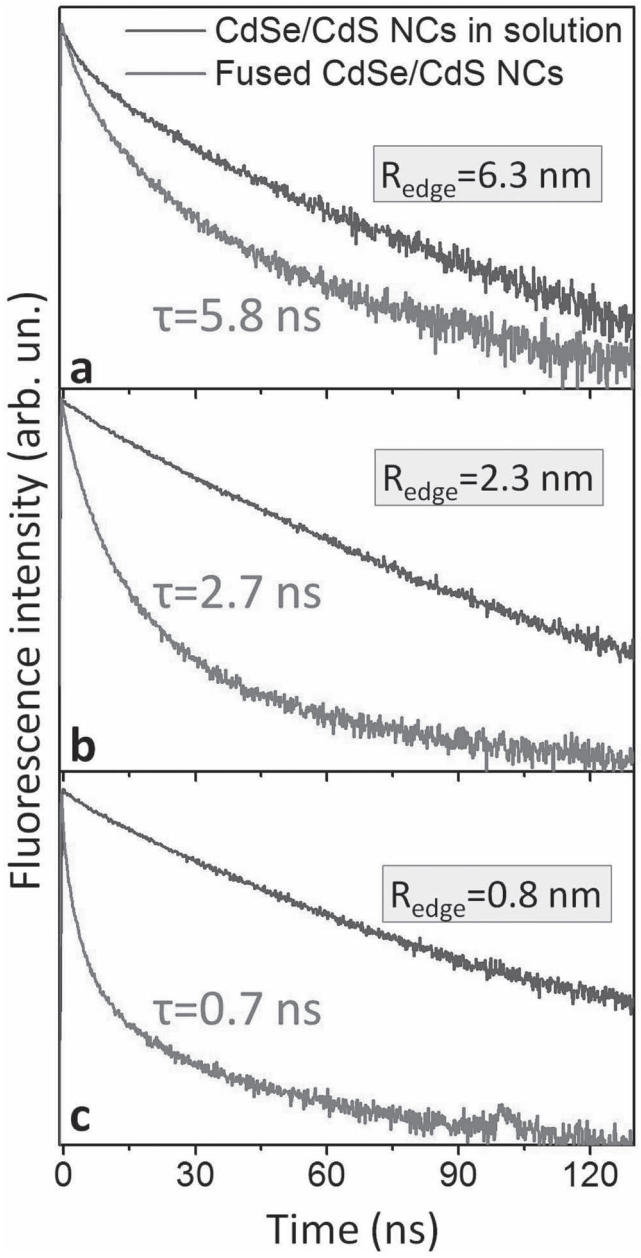

Figure 5. Comparison of the emission lifetime between isolated CdSe/CdS NCs in solution (blue curve) and CdS-encapsulated CdSe NC arrays fabricated *via* crystallographic fusion of core/shell NCs (red curve). (a) FL lifetime of 10.26-nm CdSe/CdS NCs in toluene (blue) and CdS-encapsulated CdSe NC solids with R_{edge} of 6.3 nm. (b) FL lifetime of 6.32-nm CdSe/CdS NCs in toluene (blue) and CdS-encapsulated CdSe NC solids with R_{edge} of 2.3 nm (red). (c) FL lifetime of 4.77-nm CdSe/CdS NCs in toluene (blue) and CdS-encapsulated CdSe NC solids with R_{edge} of 0.8 nm (red).

approximation, the rate of CdSe-to-CdSe or CdSe-to-surface charge tunneling, β/h, is expected to subside exponentially with R_{edge}. Assuming that the tunneling process is the second dominant contribution into the decay of excitons in CdSe NCs besides the radiative channel, we can then express the emission quantum yield as a function of R_{edge},

Table 1. The summary of optical characteristics for isolated CdSe/CdS core/shell NCs in solution and CdS-encapsulated CdSe NC solids.

CdSe shell thickness [nm]	R_{edge}, [2*H]	Solid filling factor [%]	FL lifetime in solution[ns]	FL lifetime in a solid [ns]	CdSe FL QY in a matrix [%]
4.83	9.67	1.3	36.8	23.2	43.9
4.12	8.24	1.8	30.3	16.1	30.5
3.13	6.26	3.1	13.4	10.95	20.2
2.55	5.1	4.4	24.0	8.35	14.1
1.16	2.33	13.2	22.1	2.7	5.0
0.38	0.77	30.1	18.8	0.7	1.4

$$QY = \frac{1}{1+\beta(R_{edge})/h\Gamma_R} = \frac{1}{1+x\exp(-\alpha R_{edge})} \quad (2)$$

where Γ_R is a radiative rate, x is a dimensionless parameter, $\alpha = 2(2m^*\Delta E/h^2)^{1/2}$, and β is given by Equation 1. By varying the parameter x in Equation 2, we were able to fit the R_{edge} dependence of the experimental emission QY for CdSe/CdS solids (**Figure 6**). The comparison of model calculations (red curve) with the experimental data (open circles) reveals a fairly close fit, indicating that exponential tunneling is indeed the main mechanism limiting the FL quantum yield in CdSe/CdS solids. This is an important result which suggests that other de-excitation pathways in CdSe, such as charge trapping on lattice defects or scattering at heteroepitaxial boundaries, do not play a significant role in carrier decay.

When the matrix medium consists entirely of CdS semiconductor, the height of the potential barrier, ΔE, is only ≈0.1 eV for electrons and ≈0.4 eV for holes (see Figure 2a), such that

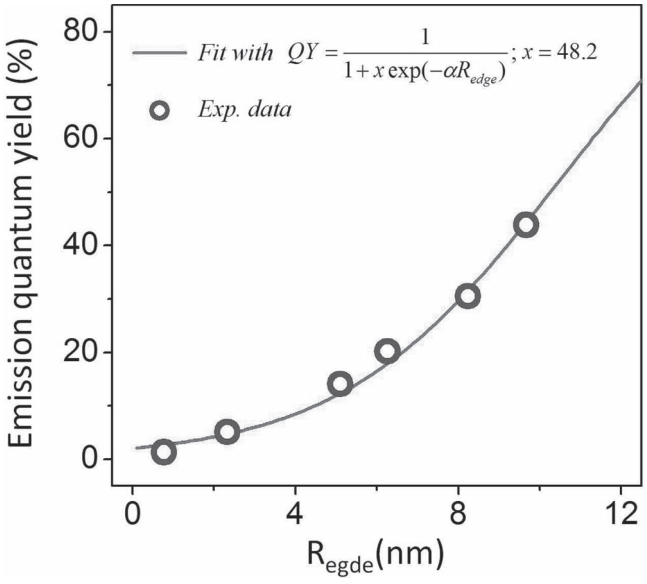

Figure 6. Fit of the experimental emission QY (blue circules) of inter-fused CdSe/CdS NCs with a model curve, given by Equation 2. The best fit is obtained for x = 48.2.

a near-complete suppression of interparticle charge transfer ($\beta/h \rightarrow 0$) is achieved only when R_{edge} is greater than 10 nm. On the other hand, matrices that employ a few monolayers of ZnS (ΔE_e = 1.1 eV, ΔE_h = 0.5 eV) in addition to CdS, make it possible to obtain the emission quantum yield in the 45–52% range with R_{edge} as little as 3.4 nm (QY = 45%), which corresponds to a filling factor of 8.2%. The observed QYs for ZnS-terminated matrices compare favorably to those of previously reported titania-incorporated CdSe NC films for which the corresponding QY values did not exceed 15%.[26]

Improving the thermal stability of NC films is important for their deployment in light-emitting devices, as many of those applications are subject to the generation of heat. In organic-capped NC solids, a complete thermal sintering occurs at relatively low temperatures. In SMENA films the presence of heteroepitaxial bonding between NC surfaces and the matrix semiconductor is expected to prevent a low-temperature oxidation process, deferring the thermal degradation of NCs to occur only at higher temperatures *via* the phase transition of the lattice.[33] Here, we test this hypothesis by comparing the thermal stability of CdSe NCs incorporated into CdS matrices with that of organically-capped CdSe NC films. To this end, the effect of the substrate temperature on the intensity of band edge emission in both films was compared. According to **Figure 7**, heating of (b) matrix-encapsulated and (c) ligand-capped CdSe NCs in inert atmosphere results in eventual suppression of the emission, which was taken as a sintering temperature of CdSe. In the case of CdSe NCs encapsulated with ≈3.15 nm of CdS shell, the sintering temperature was 90–100 °C above that of organic-capped CdSe NC solids. More importantly, the width of the emission peak in SMENA remained roughly constant during the heat exposure, indicating that the carrier localization was preserved in CdSe NCs embedded into CdS matrices. These experiments demonstrate an enhanced heat resistance of CdSe SMENA solids as compared to organic-interlinked NC films.

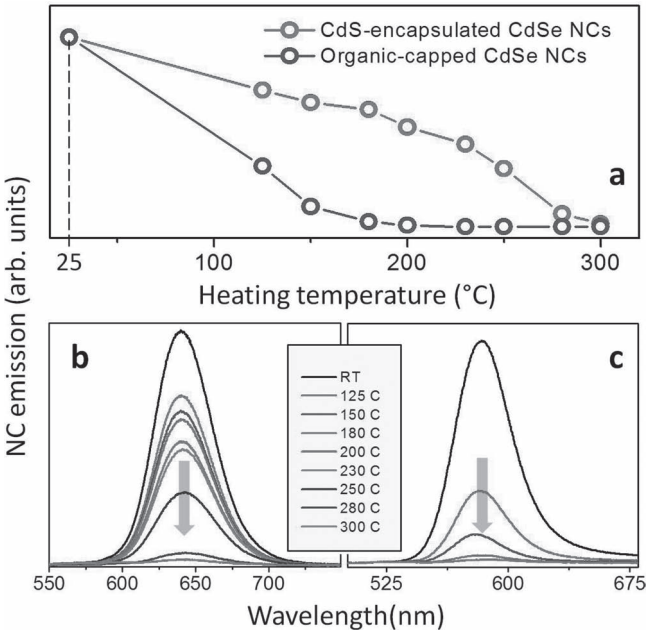

Figure 7. (a) Comparison of the thermal stability of organic-capped (blue) and CdS-encapsulated (red) CdSe NC arrays. (b,c) Temperature dependence of the band-edge emission peak area for CdS-encapsulated CdSe NC arrays (R_{egde} ≈ 6.3 nm) in (b), and organic-capped CdSe NC films (c).

3. Conclusions

In summary, a novel strategy for the integration of semiconductor NCs into transparent host matrices deployable for solid-state optical applications is presented. The method relies on heteroepitaxial inclusion of CdSe NCs into matrices of wide band gap CdS or graded $Cd_xZn_{1-x}S$/ZnS semiconductors, which preserve the quantum confinement of excited carriers resulting in emission quantum yields of up to 52%. The use of an all-inorganic film architecture also boosts the stability of incorporated CdSe NCs, giving rise to air-stable NC solids showing a compelling heat resistance. In addition to increased fluorescence QY and long-term stability, fabricated NC films exhibit a high refractive index ranging from 1.8 to 2.2, which should avail their utilization in wave-guided light-emitting devices.

4. Experimental Section

Materials: Sulfur (99.999%, Acros), 1-Octadecene (ODE, tech., 90%, Aldrich), Cadmium oxide (CdO, 99.99%, Aldrich), Octadecylamine (ODA, 90%, Fisher), Oleic acid (OA, tech., 90%, Aldrich), Stearic acid (SA, 97%, ACROS), Tri-n-octylphosphine (TOP, 97%, Strem), Tributylphosphine (TBP, 97%), Diphenyl ether (DPE, 99%, Alfa Aesar), Hexamethyldisilathiane (TMS, Aldrich), Tri-n-octylphosphine oxide (TOPO, 99%, Aldrich), n-Octadecylphosphonic acid (ODPA, 98%, PCI Synthesis), n-Hexylphosphonic acid (HPA, 98%, PCI Synthesis), Potassium hydroxide (KOH, pellets, Acros), Hexadecylamine (HDA, tech,, Fluke), 11-Mercaptoundecanoic acid (MUA, 95%, Aldrich), Diethylzinc (Et_2Zn, 15% wt., 1.1 M solution in toluene, Aldrich), Selenium powder (Se, 200 mesh, Acros), Cadmium acetate dihydrate($(CH_3COO)_2Cd$, 98%, Acros), Zinc acetate dihydrate ($(CH_3COO)_2Zn$, 98%, Acros), Hexane (anhydrous, 95%, Aldrich), Methanol (anhydrous, 99.8%, Aldrich), Ethanol (anhydrous, 95%, Aldrich), Sodium sulfide nonanhydrate ($Na_2S.9H_2O$, 98% Alfa Aesar), 3-Mercaptopropionic acid (3-MPA, 99% Alfa Aesar), Tert-butanol (99.7%, Aldrich), and Toluene (anhydrous, 99.8%, Aldrich) were used as purchased. All reactions were performed under argon atmosphere using the standard air free Schlenk technique unless otherwise stated.

Synthesis of CdSe seeds: To grow 4.0-nm CdSe NCs, CdO (0.0256 g), stearic acid (0.2275 g), and ODE (2.53 mL) were combined in a 50 mL three-neck flask, then heated to 200 °C under argon to dissolve CdO. The solution was then cooled to room temperature, at which point ODA (1.5 g) and TOPO (0.5 g) were added to the flask. Under argon flow, this mixture was then reheated to 280 °C. When this temperature was reached, a selenium solution, prepared under argon by dissolving Se (0.1579 g) *via* sonication in TBP (0.58 mL) and further diluting it with ODE (1.73 mL), was quickly injected. After 3–4 min of growth time, the solution containing CdSe NCs with an absorption peak at 585 ± 3 nm were obtained. At this point, the flask was raised from the heating mantle and upon cooling of the reaction mixture to room temperature, chloroform (6 mL) were added. The contents of the reaction flask were then distributed in two tubes and centrifuged. The precipitate was discarded while the reddish clear solution was mixed with acetone (8 mL) and centrifuged again. At this point all nanocrystals precipitated and were subsequently re-dissolved in chloroform (3–4 ml).

Synthesis of CdSe/CdS core/shell NCs: Synthesis of CdSe/CdS core/shell NCs with a shell thickness ranging from 1 to 15 monolayers (MLs) was performed using an "accelerated" procedure evolved from

a previously reported seeded-type growth approach.[42] In a typical synthesis, S (0.120 g) was dissolved in TOP (1.81 mL) at 200 °C, and after cooling down to room temperature was mixed with CdSe nanocrystal solution in chloroform (toluene) (1 mL). The concentration of CdSe NCs in 1 mL of solvent determines the thickness of the resulting CdS shell. For instance, if the absorption of 100 times diluted CdSe solution was in the 0.3–0.4 range (at the excitonic peak), the resulting shell was 3–5 MLs thick. Decreasing the concentration, such that the absorbance of 100 times diluted solution was 0.2 lead to the formation of thicker shells (H = 10–15 MLs). Conversely, increasing the concentration of CdSe seed NCs (A > 0.5) promoted the growth of thin shells (H = 1–3 MLs). Separately, a mixture of CdO (0.060 g), TOPO (3.0 g), ODPA (0.290 g), and HPA (0.080 g) in a 50 mL 3-neck flask was exposed to vacuum at 150 °C for ca. 30 min. Subsequently, the system was switched to Ar flow and heated to 300 °C until the solution turned optically clear and colorless. At this point, TOP (0.9 mL) was added to the flask and the temperature was raised to 320 °C. The growth of the CdS shell was initiated with a swift injection of nanocrystal seeds/sulfur mixture at 320 °C. After the initial temperature drop, the reaction temperature was allowed to recover to 300 ºC. The overall growth time was 6–7 min. Purification of the CdSe/CdS NCs was carried out by precipitation with ethanol, and re-disolution with chloroform. This process was repeated two times and the final product was stored in chloroform.

Growth of the ZnS shell onto CdSe/CdS core/shell NCs: In a typical synthesis, a mixture of TOP (5 mL), OA (1 mL), DPE (10 mL), and CdSe/CdS (10 mg) core/shell NCs in chloroform was heated under argon to 120 ºC. When the solvent had evaporated, an injection of a previously prepared sulfur solution (0.52 mL), comprising thorougly degassed TOP (2 mL) and TMS (0.6 ml), was made. This was immediately followed by an injection of a 10% solution of diethyl zinc in hexane (0.1 mL). S and Zn injections were then continuously administered every 10 min until all of the S solution had been exhausted. CdSe/CdS/ZnS core/shell/shell NCs were purified in a similar manner as CdSe/CdS core/shell NCs.

MUA Ligand exchange: The original hydrophobic ligands on CdSe were exchanged with hydrophilic MUA molecules using a method reported by Costi et al.[54] To this end, the solution of NCs in chloroform (10–12 mL) was mixed with MUA (10 mg). Subsequently, solution of KOH in ultrapure water (4 mL, C = 0.09M) was added, and the mixture was vigorously shaken until NCs were transferred into the aqueous phase. The latter was separated and extracted one more time using aqueous KOH (2 mL). Finally, MUA-capped NCs were precipitated with methanol (10 mL) and re-dissolved in ultrapure water (4 mL).

Fabrication of CdS-encapsulated CdSe NC films (SMENA films): All steps were performed inside the glovebox. Typically, 4–5 drops of CdSe/CdS NCs in octane with a concentration of 2–5 mg/mL were placed onto a still glass slide and allowed to spread until it covered the substrate. The NC solution was left to soak until the center started to dry, then spun at 2500 RPM for 10–15 seconds. Next, 10 drops of a 1:3 MPA/methanol solution were placed on the film fully covering the surface, and then spun at 2500 RPM for 15 seconds. The film was then washed with 10 drops of methanol, spun at 2500 RPM until dry, then washed once again with 10 drops of octane in the same manner. The film was annealed at 150 °C for 15 minutes after every three layers. Overall, 8–10 layers were needed to form a 300-nm SMENA film.

In-filling of SMENA pores with CdS (ZnS): To deposit CdS into the pores of an annealed, all-inorganic CdSe/CdS film, a SILAR method was employed. A cadmium bath was prepared by dissolving cadmium acetate (0.43 g) in methanol (80 mL). The sulfur bath was made by combining of $Na_2S{\cdot}9H_20$ (0.38 g) with methanol (80 mL). The sample was placed in the cadmium bath for 1 minute, rinsed with methanol for 1 minute, placed in the sulfur bath for 1 minute, then finally washed in methanol again. This process was repeated 2–16 times, depending on the desired number of CdS monolayers. The film was then annealed at 150 °C for 15 minutes. For in-filling with ZnS, zinc acetate (0.34 g) in methanol (80 mL) were used in place of Cd.

Characterization: UV-vis absorption and photoluminescence spectra were recorded using CARY 50 scan spectrophotometer and Jobin Yvon Fluorolog FL3-11 fluorescence spectrophotometer. High resolution transmission electron microscopy measurements were carried out using JEOL 311UHR operated at 300 kV. Specimens were prepared by depositing a drop of nanoparticle solution in organic solvent onto a carbon-coated copper grid and allowing it to dry in air. X-ray powder diffraction (XRD) measurements were carried out on a Scintag XDS-2000 X-ray powder diffractometer. FL lifetime measurements were performed using a time-correlated single photon counting setup utilizing SPC-630 single-photon counting PCI card (Becker & Hickle GmbH), picosecond diode laser operating at 400 nm as an excitation source (Picoquant), and id50 avalanche photodiode (Quantique).

Measurements of the film refractive index: The thickness of the nanoparticle film before and after the pore in-filling step was done using a Cauchy model. The *psi* and *delta* values were obtained from a variable angle, monochromatic ellipsometer. The wavelength used was 632.8 nm. Each measurement was carried with at least three angles. The ellipsometer is a PhE-101 discrete wavelength from Angstrom Advanced Inc. The iterations for the Cauchy exponential model were carried out in the Angstrom Advanced Inc PhE102 software. The models were fit to *delta* and *psi* and the same time. The number of steps for each iteration was a maximum of 250 with a tolerance of 0.1.

Fluorescence quantum yield measurements: The FL quantum yield of both colloidal and solid NC samples was determined relative to organic dyes with known emission efficiencies using the following equation:

$$QY_{NC} = QY_{Dye}\frac{I_{NC}}{I_{Dye}}\left(\frac{n_{NC}}{n_{Dye}}\right)^2\frac{1-10^{-A_{Dye}}}{1-10^{-A_{NC}}}$$

where I is the spectrally integrated fluorescence, n is the refractive index of the sample (which for solid samples was measured using a Cauchy model at 632 nm and extrapolated down to the excitation wavelength of 532 nm), and A is the optical absorbance of the sample at the excitation wavelength. The NC samples were exited using a 532-nm monochromatic laser (GS3230-20). Rhodamine B dye in ethanol with the emission at $\lambda = 610$ nm was used as a reference for QY measurements. The FL was detected using a home-built system comprising Shamrock spectrograph and Andor Newton EMCCD camera.

Note: X-ray power diffraction data (XRD), additional TEM images and FTIR spectra are available in the Supporting Information.

Supporting Information

Supporting Information is available from the Wiley Online Library or from the author.

Acknowledgements

We gratefully acknowledge OBOR "Material Networks" program and Bowling Green State University for financial support. This work was partly supported by the NSF under Award CHE - 1112227.

Received: April 3, 2012
Published online: May 11, 2012

[1] S. Coe, W. K. Woo, M. Bawendi, V. Bulovic, *Nature* **2002**, *420*, 800.
[2] N. Tessler, V. Medvedev, M. Kazes, S. H. Kan, U. Banin, *Science* **2002**, *295*, 1506.
[3] J. S. Steckel, P. Snee, S. Coe-Sullivan, J. R. Zimmer, J. E. Halpert, P. Anikeeva, L. A. Kim, V. Bulovic, M. G. Bawendi, *Angew Chem. Int. Ed.* **2006**, *45*, 5796.
[4] V. L. Colvin, M. C. Schlamp, A. P. Alivisatos, *Nature* **1994**, *370*, 354.
[5] M. C. Schlamp, X. G. Peng, A. P. Alivisatos, *J. Appl. Phys.* **1997**, *82*, 5837.

[6] H. Mattoussi, L. H. Radzilowski, B. O. Dabbousi, E. L. Thomas, M. G. Bawendi, M. F. Rubner, *J. Appl. Phys.* **1998**, *83*, 7965.
[7] Q. Sun, A. Y. Wang, L. S. Li, D. Wang, T. Zhu, J. Xu, C. Yang, Y. Li, *Nat. Photonics* **2007**, *1*, 717.
[8] J. M. Caruge, J. E. Halpert, V. Wood, V. Bulovic, M. G. Bawendi, *Nat. Photonics* **2008**, *2*, 247.
[9] V. Wood, M. J. Panzer, J. M. Caruge, J. E. Halpert, M. G. Bawendi, V. Bulovic, *Nano Lett.* **2010**, *10*, 24.
[10] M. Kazes, D. Y. Lewis, Y. Ebenstein, T. Mokari, U. Banin, *Adv. Mater.* **2002**, *14*, 317.
[11] V. I. Klimov, A. A. Mikhailovsky, S. Xu, A. Malko, J. A. Hollingsworth, C. A. Leatherdale, H. Eisler, E. H. Bawendi, *Science.* **2000**, *290*, 314.
[12] S. I. Shopova, G. Farca, A. T. Rosenberger, W. M. S. Wickramanayake, N. A. Kotov, *Appl. Phys. Lett.* **2004**, *85*, 6101.
[13] J. N. Cha, M. H. Bartl, M. S. Wong, A. Popitsch, T. J. Deming, G. D. Stucky, *Nano Lett.* **2003**, *3*, 907.
[14] V. I. Klimov, *J. Phys. Chem. B.* **2006**, *110*, 16827.
[15] V. C. Sundar, H. J. Eisler, M. G. Bawendi, *Adv. Mater.* **2002**, *14*, 739.
[16] V. I. Klimov, S. A. Ivanov, J. Nanda, M. Achermann, I. Bezel, J. A. McGuire, A. Piryatinski, *Nature.* **2007**, *447*, 441.
[17] D. V. Vezenov, B. T. Mayers, R. S. Conroy, G. M. Whitesides, P. T. Snee, Y. Chan, D. G. Nocera, M. G. Bawendi, *J. Am. Chem. Soc.* **2005**, *127*, 8952.
[18] P. G. Van Patten, *J. Phys. Chem. C.* **2008**, *112*, 10622.
[19] R. H. Friend, R. W. Gymer, A. B. Holmes, J. H. Burroughes, R. N. Marks, C. Taliani, D. D. C. Bradley, D. A. Dos Santos, J. L. Bredas, M. Logdlund, W. R. Salaneck, *Nature* **1999**, *397*, 121.
[20] H. Morkoc, S. Strite, G. B. Gao, M. E. Lin, B. Sverdlov, M. B. Burns, *J. Appl. Phys.* **1994**, *76*, 1363.
[21] J. J. Jasieniak, J. Padicifico, R. Signorini, A. Chiasera, M. Ferrari, A. Martucci, P. Mulvaney, *Adv. Funct. Mater.* **2007**, *17*, 1654.
[22] L. Pang, Y. Shen, K. Tetz, Y. Fainman, *Opt. Express* **2005**, *13*, 44.
[23] I. Suárez, H. Gordillo, R. Abargues, S. Albert, J. Martínez-Pastor, *Nanotechnology* **2011**, *22*, 435202.
[24] M. Wang, M. Zhang, J. Qian, F. Zhao, L. Shen, G. Scholes, M. Winnik, *Langmuir* **2009**, *25*, 11732.
[25] V. C. Sundar, H. J. Eisler, M. G. Bawendi, *Adv. Mater.* **2002**, *14*, 739.
[26] M. A. Petruska, A. V. Malko, P. M. Voyles, V. I. Klimov, *Adv. Mater* **2003**, 610.
[27] L. Qu, X. Peng, *J. Am. Chem. Soc.* **2002**, *124*, 2049–2055.
[28] H. Tetsuka, T. Ebina, F. Mizukami, *Adv. Mater.* **2008**, *20*, 3039.
[29] M. Miri Kazes, T. Saraidarov, R. Reisfeld, U. Banin, *Adv. Mater.* **2009**, *21*, 1716.
[30] B. Liu, T. Ren, J. R. Zhang, H. Y. Chen, J. J. Zhu, C. Burda, *Electrochem. Commun.* **2007**, *9*, 551.
[31] M. V. Kovalenko, R. D. Schaller, D. Jarzab, M. A. Loi, D. V. Talapin, *J. Am. Chem. Soc.* **2012**, DOI: 10.1021/ja2087689.
[32] J. W. Stouwdam, J. Shan, F. C. J. M. Van Veggel, A. G. Pattantyus-Abraham, J. F. Young, M. Raudsepp, *J. Phys. Chem. C.* **2007**, *111*, 1086.
[33] E. Kinder, P. Moroz, G. Diederich, A. Johnson, M. Kirsanova, A. Nemchinov, T. O'Connor, D. Roth, M. Zamkov, *J. Am. Chem. Soc.* **2011**, *133*, 20488.
[34] B. Mashford, J. Baldauf, T. L. Nguyen, A. M. Funston, P. Mulvaney, *J. Appl. Phys.* **2011**, *109*, 094305.
[35] Z. A. Peng, X. G. Peng, *J. Am. Chem. Soc.* **2001**, *123*, 183.
[36] J. H. Fendler, *Chem. Mater.* **1996**, *8*, 1616.
[37] H. M. Pathan, C. D. Lokhande, *Bull. Mater. Sci.* **2004**, *27*, 85.
[38] J. J. Li, Y. A. Wang, W. Guo, J. C. Keay, T. D. Mishima, M. B. Johnson, X. Peng, *J. Am. Chem. Soc.* **2003**, *125*, 12567.
[39] W. G. J. H. M. Van Sark, K. W. J. Barnham, L. H. Slooff, A. J. Chatten, A. Büchtemann, A. Meyer, S. J. McCormack, R. Koole, D. J. Farrell, R. Bose, E. E. Bende, A. R. Burgers, T. Budel, J. Quilitz, M. Kennedy, T. Meyer, C. De Mello Donegá, A. Meijerink, D. Vanmaekelbergh, *Opt. Express* **2008**, *16*, 21773.
[40] R. Y. Wang, R. Tangirala, R. Raoux, J. L. Jordan-Sweet, D. J. Milliron, *Adv. Mater.* **2012**, *24*, 99.
[41] Y. Chen, J. Vela, H. Htoon, J. L. Casson, D. J. Werder, D. A. Bussian, V. I. Klimov, J. A. Hollingsworth, *J. Am. Chem. Soc.* **2008**, *130*, 5026.
[42] L. Carbone, C. Nobile, M. De Giorgi, F. Della Sala, G. Morello, P. Pompa, M. Hytch, E. Snoeck, A. Fiore, I. R. Franchini, *Nano Lett.* **2007**, *7*, 2942.
[43] N. N. Hewa-Kasakarage, M. Kirsanova, A. Nemchinov, N. Schmall, P. Z. El-Khoury, A. N. Tarnovsky, M. Zamkov, *J. Am. Chem. Soc.* **2009**, *131*, 1328.
[44] X. Chen, Y. Lou, B. Clemens, *Int. J. Nanotechnol.* **2004**, *1*, 105.
[45] A. Sitt, F. Della Sala, G. Menagen, U. Banin, *Nano Lett.* **2009**, *9*, 3470.
[46] S. S. Lo, T. Mirkovic, C. H. Chuang, C. Burda, G. D. Scholes, *Adv. Mater.* **2011**, *23*, 180.
[47] Y. Wang, N. Herron, *J. Phys. Chem.* **1991**, *95*, 525.
[48] J. M. Luther, M. Law, M. C. Beard, Q. Song, M. O. Reese, R. J. Ellingson, A. J. Nozik, *Nano Lett.* **2008**, *8*, 3488.
[49] K. P. Acharya, H. Khatri, S. Marsillac, B. Ullrich, P. Anzenbacher, M. Zamkov, *Appl. Phys. Lett.* **2010**, *97*, 201108.
[50] K. P. Acharya, R. S. Khnayzer, T. O'Connor, G. Diederich, M. Kirsanova, A. Klinkova, D. Roth, E. Kinder, M. Imboden, M. Zamkov, *Nano Lett.* **2011**, *11*, 2919.
[51] W. W. Yu, E. Chang, R. Drezek, V. L. Colvin, *Biochem. Biophys. Res. Commun.* **2006**, *348*, 781.
[52] S. F. Wuister, C. De Mello Donegá, A. Meijerink, *J. Phys. Chem. B.* **2004**, *108*, 17393.
[53] R. E. Chandler, A. J. Houtepen, J. Nelson, D. Vanmaekelbergh, *Phys. Rev. B.* **2007**, *75*, 085325.
[54] R. Costi, A. E. Saunders, E. Elmalem, A. Salant, U. Banin, *Nano Lett.* **2008**, *8*, 637.